RSC Advances

PAPER

View Article Online
View Journal | View Issue

Cite this: *RSC Adv.*, 2024, **14**, 20982

Monitoring alterations of all-*trans*-retinal in human brain cancer cells by label-free confocal Raman imaging: regulation of the redox status of cytochrome *c*†

Karolina Jarczewska, Monika Kopeć, Halina Abramczyk and Jakub Maciej Surmacki *

Received 28th February 2024
Accepted 26th June 2024

DOI: 10.1039/d4ra01542h

rsc.li/rsc-advances

This article has shown the impact of all-*trans*-retinal on human brain cancer, which is apparent in the shifts in the redox status of cytochrome *c* in a single cell. The connection between cytochrome *c* expression and its role in cancer development remains relatively unexplored. To assess this, we employed Raman spectroscopy and imaging to determine the redox state of the iron ion in cytochrome *c* across different cellular locations, including mitochondria, cytoplasm, lipid droplets, and the endoplasmic reticulum within human brain cancer cells. We have analyzed normal human astrocytes (NHA) and two brain cancer cell lines (astrocytoma – CRL-1718 and glioblastoma – U-87 MG) without and supplemented with all-*trans*-retinal. Our results confirmed that human brain cancer cells demonstrate varying redox status compared to normal cells based on the established correlation between the intensity of the cytochrome *c* Raman band at 1583 cm^{-1} and the malignancy grade of brain cancer cells. Our research unveiled that all-*trans*-retinal induces remarkable changes in the mitochondrial functional activity (redox status) of cancer cells, which were measured by confocal Raman spectroscopy and imaging.

Introduction

Cancer is a disease characterized by the abnormal mutation of previously healthy cells, leading to uncontrolled growth, the stimulation of angiogenesis and the ability to spread to other tissues. Brain cancer primarily affects patients aged 50 to 65, although more than 15% of those affected are individuals under 18 years old.[1] The presence of a brain tumor results in a reduction in intracranial space, thereby exerting pressure on the remaining brain structures. The treatment of brain tumors involves options like surgery, radiation therapy, chemotherapy, steroid therapy, or a combination of these therapeutic approaches. Surgery, including craniotomy, can lead to the complete removal of select tumors in certain cases.

A wide range of brain cancer types exists, with primary tumors originating from various sources, including glial cells, meninges, choroid plexus, the pineal gland, the pituitary gland, or blood vessels. These types encompass glioblastomas, gliomas, and meningiomas. It is worth noting that nearly half of all brain cancers result from metastases. However, the blood–brain barrier restricts the entry of drugs into the brain, which poses a challenge to the effective treatment of brain tumors.[2–4]

The maintenance of homeostasis relies on the delicate balance of various compounds present in the human body. Any disruption of this balance can lead to the emergence of diseases, especially cancer. Carcinogenesis disrupts this equilibrium and leads to alterations in the levels of specific compounds within metabolic pathways. For example, the levels of retinoids, including retinal, may differ from those in normal cells. By controlling these changes, such as significantly increasing or decreasing the quantity of a specific compound crucial for a metabolic pathway, it becomes feasible to impede a particular stage of carcinogenesis.[5]

Carotenoids and retinoids constitute two categories of nutritionally significant compounds, with carotenoids being present in a variety of plant-based foods and retinoids primarily found in animal-derived sources. The levels of these compounds in human individuals depend on the diversity and quantity of their dietary intake. Some carotenoids and retinoids have been the subject of investigation regarding their beneficial effects in the prevention of many major diseases and their influence on the immune system. It has been observed that retinoids have the potential to mediate or trigger processes like cell proliferation, differentiation, immune modulation, and the maintenance of the epidermal barrier.[6]

Lodz University of Technology, Faculty of Chemistry, Institute of Applied Radiation Chemistry, Laboratory of Laser Molecular Spectroscopy, Wroblewskiego 15, 93-590 Lodz, Poland. E-mail: jakub.surmacki@p.lodz.pl; Tel: +48 426313188

† Electronic supplementary information (ESI) available. See DOI: https://doi.org/10.1039/d4ra01542h

Classified within the retinoids group, retinal is an aldehyde and serves as an active form of vitamin A, displaying properties that place between retinol and retinoic acid. A retinal requires one transformation to retinoic acid in human skin. This compound impacts skin physiology by transforming into retinoic acid, which binds to receptors, instigating the renewal process and acting as an anti-aging agent. Retinal offers a range of activities, including epidermal exfoliation, melanin transport inhibition and the stimulation of collagen and elastin synthesis.[7] Retinal's central role is in the visual process, where it participates in both the cone visual cycle and the canonical visual cycle. All-*trans*-retinal is an integral part of these cycles.[8] Nevertheless, it is worth noting that an excessive concentration of retinoids, such as retinal, can have detrimental health effects, potentially leading to conditions like retinitis pigmentosa.[9]

Carotenoid metabolism generates retinoids *in vivo* and *in vitro*.[10] Fig. 1 shows the mechanism of metabolism of β-carotene to retinol and retinoic acid and representative Raman spectra of β-carotene, all-*trans*-retinal, retinoic acid and retinol. In the first step, all-*trans*-retinal is generated from β-carotene by oxidative cleavage of $C_{15}/C_{15'}$ double bonds. This cleavage is catalyzed by carotenoid-cleaving enzyme (CCE) 15,15′-monooxydase BCMO1, which is localized in the cytoplasm.[11] The second step is that the retinal might undergo oxidation or reduction on the aldehyde end to give all-*trans*-retinoic acid or all-*trans*-retinol respectively.[8] Retinal might be metabolized in the liver to retinoic acid by retinaldehyde dehydrogenase or CYP from the cytochrome P450 family. Alcohol dehydrogenase might transform retinal back to retinol, thus this reaction is reversible. Retinoids act by binding to receptors located in the cell nucleus. Expression of these receptors differs depending on part of the body. Retinoid receptors are located exclusively in the epidermis, hair follicles, sebaceous glands, or cells of the immune system. The amount of receptors in these cells depends on their condition. If there is an inflammation in the cell, the number of receptors increases.[12]

To understand the involvement of retinoids in cellular signal transduction in cancer, it is essential to utilize the right techniques for *in vivo* retinoid sensing, enabling the monitoring of retinoid distribution and temporal changes in cells and tissues. Raman spectroscopy and imaging emerge as valuable tools, providing not only a biochemical profile of cells and tissues but also a deeper understanding of disease progression.

Raman spectroscopy is an analytical approach rooted in the phenomenon of spontaneous and nonlinear Raman scattering, which occurs when radiation interacts with a molecule.[13,14] This interaction leads the molecule to enter a scattering virtual state, followed by the excited molecule emission. The scattered light is collected by a confocal Raman microscope and transformed into a digital signal by the detector, ultimately generating a Raman spectrum.[13,15] This technique identifies the distinctive molecular vibrations modified by the environment resulting in a spectral band broadening. The position of this band indicates the nature of the specific molecular vibration mode and its' intensity is directly proportional to the molecule's concentration.[16]

Our current understanding of retinoid metabolism in both normal and cancer brain cells is significantly limited, largely due to the absence of experimental methodologies capable of tracking retinoids within specific cell organelles in real time. The Raman-based technique outlined in this publication emerges as a valuable tool to enhance our knowledge in this field.

To address questions concerning the role of retinoids in the metabolism and signaling of brain cancer cells, we collected Raman spectra and images from brain cells exposed to redox stimuli, such as all-*trans*-retinal in *in vitro* cell culture. To accomplish this, we cultured normal human astrocytes (NHA) and two brain cancer cell lines astrocytoma (CRL-1718) and glioblastoma (U-87 MG) with all-*trans*-retinal at a concentration of 1, 10 μM during a 24 and 48 hours incubation period.

In our recent work[17] we have shown a fresh perspective on the role of retinoic acid in altering the redox state of the iron ion within the heme group of cytochrome *c*, shifting it from the oxidized Fe^{3+} to the reduced Fe^{2+} form, which carries notable implications. These implications involve the inhibition of oxidative phosphorylation, the interruption of conventional mitochondrial signal pathways that rely on specific proteins and the programmed cell death through apoptosis. The modulation of cytochrome *c*'s redox status by different retinoids may offer an appealing path for the development of potent therapeutic strategies. Consequently, our attention here is directed toward all-*trans*-retinal.

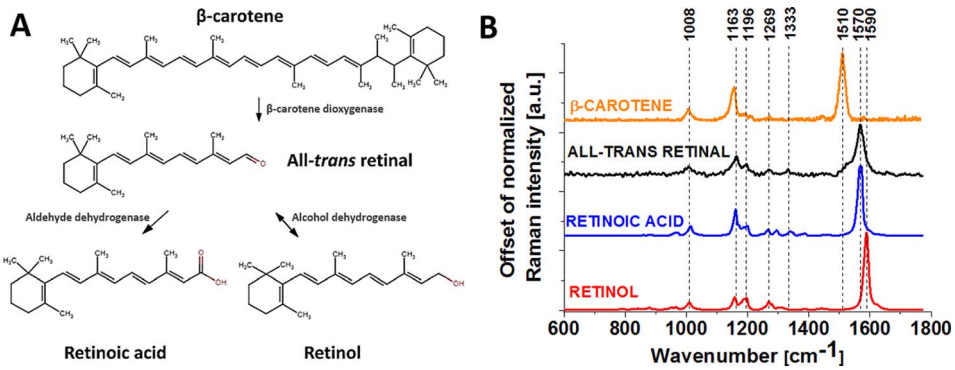

Fig. 1 Mechanism of metabolism of β-carotene (A) and Raman spectra of β-carotene, all-*trans*-retinal, retinoic acid and retinol powders (B).

Materials and methods

Chemicals

The cytochrome *c* (no. C2506), all-*trans*-retinal (no. R2500), β-carotene (no. C4582), retinoic acid (no. R2625) and retinol (no. R7632) were purchased from Merck Life Science.

Cell culture and preparation for microscopy

A normal human astrocyte (NHA) and two brain cancer cell lines astrocytoma (CRL-1718) and glioblastoma (U-87 MG) cell lines were purchased from LONZA (product number CC-2565) and ATCC, respectively. NHA was cultured first using Astrocyte Growth Medium (AGM, Lonza CC-3186) and after three

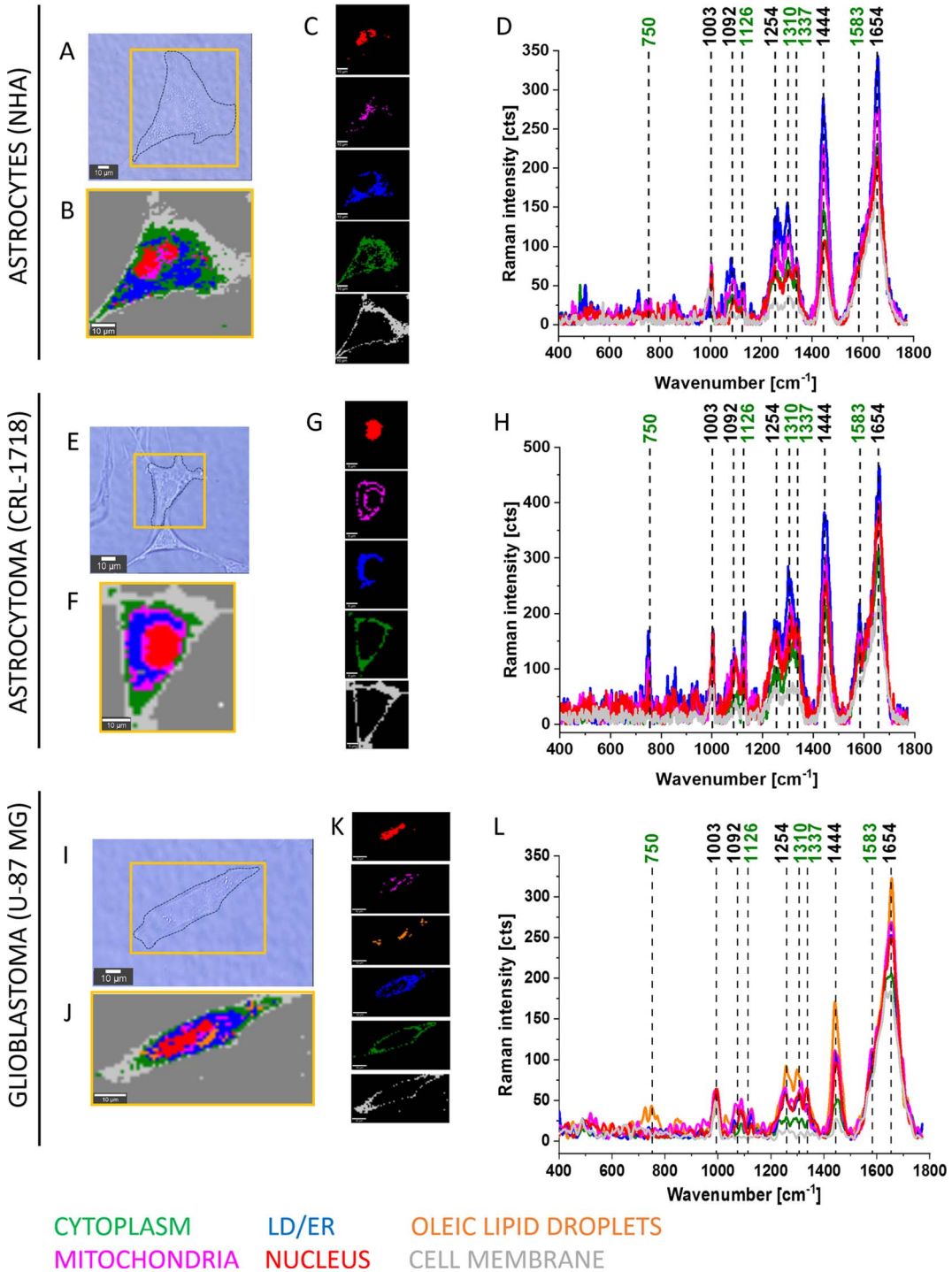

Fig. 2 Raman imaging of a typical normal human astrocyte (NHA), astrocytoma (CRL-1718) and glioblastoma (U-87 MG) cells. The microscope images (A, E and I) of the cells with Raman images (B, F and J), Raman maps of particular organelles (C, G and K) and representative Raman spectra of particular cell organelles (D, H and L): nucleus (red), mitochondria (magenta), oleic lipid droplets (orange), lipid droplets/endoplasmic reticulum (blue), cytoplasm (green), cell membrane (grey). Resolution of Raman images 1 μm, integration time 0.5 seconds, 10 mW at 532 nm.

passages the AGM was changed to a Dulbecco's Modified Eagle Medium (DMEM, Merck D0819). CRL-1718 was cultured with RPMI-1640 Medium (Merck R8758) with L-glutamine and sodium bicarbonate. U-87 MG was cultured with Minimum Essential Medium Eagle Medium – EMEM (Merck M2279). Each medium was supplemented with Fetal Bovine Serum (FBS no. 30-2020 ATCC) to a final concentration of 10%. Each medium was recharged from 2 to 3 times per week. Cells were grown in flat-bottom culture T75 flasks (TPP – Techno Plastic Products no. 90076) and maintained at 37 °C in a humidified atmosphere containing 5% CO_2. Cells were seeded on a CaF_2 window (Crystran Ltd, Poole, UK; CaF_2 Raman grade optically polished window 25 mm diameter × 1 mm thick, no. CAFP25-1R, Poole, UK) in a 35 mm Petri dish at a density of 5×10^4 cells per Petri dish the day before the examination. Before Raman examination, cells were supplemented with all-*trans*-retinal at concentrations of 1 and 10 μM for 24 and 48 hours, then fixed with 4% formalin solution (neutrally buffered) and kept in PBS (no. 10010023, Gibco) during the experiment. Each of the cell lines (NHA, CRL-1718, U-87 MG) was analyzed by Raman spectroscopy and imaging in the following variants: control – unsupplemented cells, cells supplemented with 1 μM all-*trans*-retinal for 24 and 48 hours and cells supplemented with 10 μM all-*trans*-retinal for 24 and 48 hours. This gave a total of 5 samples for each cell line. This approach aimed to be able to compare the results of supplementation depending on the dose and timing of all-*trans*-retinal.

Confocal Raman spectroscopy and imaging

Raman spectra and images were obtained using the WITec Alpha 300 RSA+ confocal microscope (Ulm, Germany). Comprehensive information regarding the WITec system is available in the provided ref. 18 The Raman spectra were

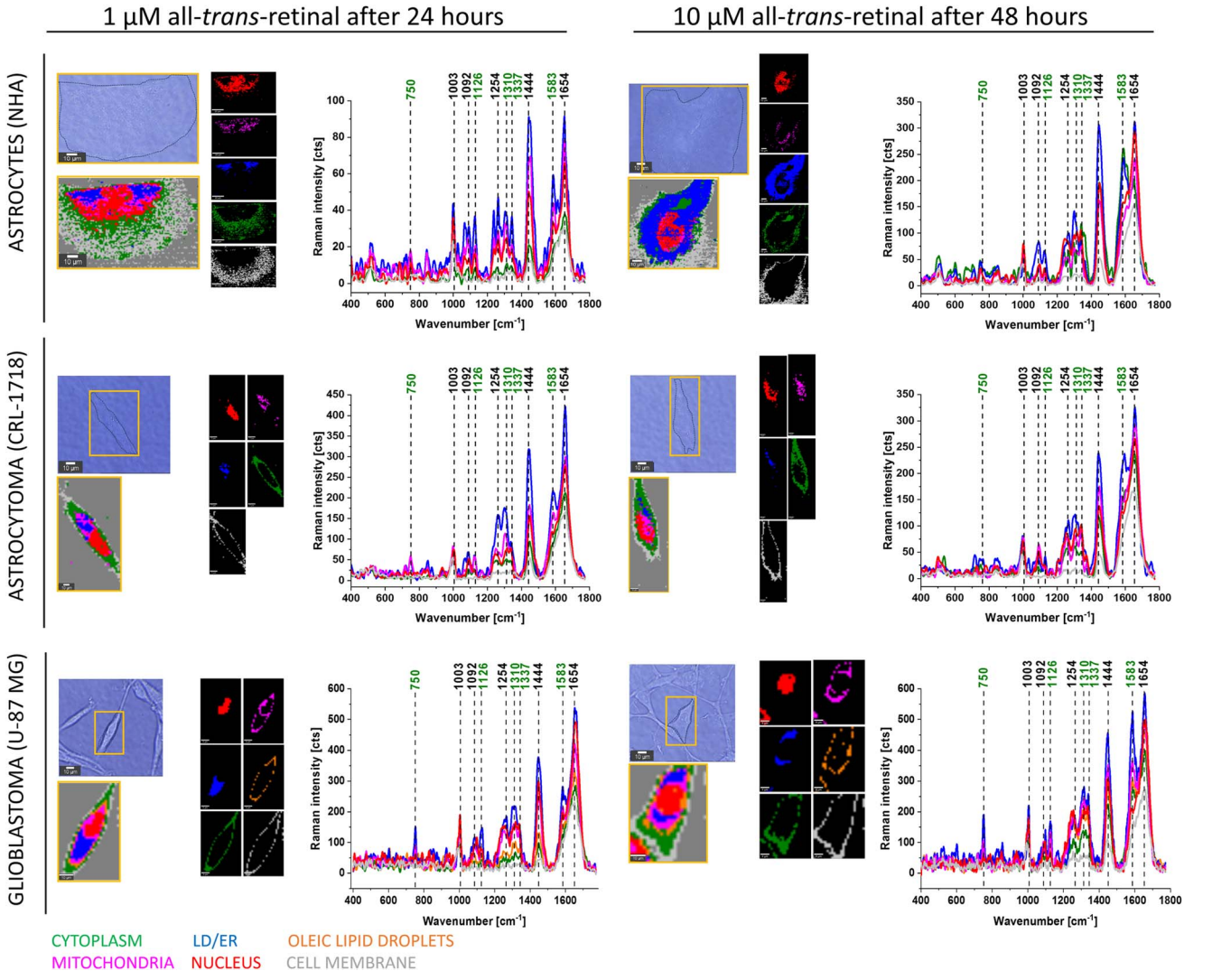

Fig. 3 Raman imaging of a typical normal human astrocyte (NHA), astrocytoma (CRL-1718) and glioblastoma (U-87 MG) cells supplemented with all-*trans*-retinal. The microscope images of the supplemented cells with Raman images and representative Raman spectra of particular cell organelles: nucleus (red), mitochondria (magenta), oleic lipid droplets (orange), lipid droplets/endoplasmic reticulum (blue), cytoplasm (green), cell membrane (grey). Data presented on the left correspond to the cells supplemented with 1 μM of all-*trans*-retinal for 24 hours and on the right part – with 10 μM of all-*trans*-retinal for 48 hours. Resolution of Raman images 1 μm, integration time 0.5 seconds, 10 mW at 532 nm.

measured with a 532 nm excitation wavelength laser with the power of 10 mW in the focus spot and with an integration time of 0.3 seconds (2300–3700 cm^{-1}) and 0.5 seconds (0–1800 cm^{-1}) by CCD camera in enhanced mode (EMCCD). The objective used is a Nikon with a 40× magnification, a numerical aperture (NA = 1.0) and a water solutions measurement cap. Raman images were recorded with a spatial resolution of 1 × 1 μm. A typical Raman map of a single cell consists of 1200 Raman spectra (map size 30 × 40 μm). Raman data analysis was performed using WITec (WITec Project Plus 4) and OriginPro 2021 programs. Raman imaging data were analyzed by the Cluster Analysis method described in our previous papers.[18,19] The number of clusters was 7, the minimum number of clusters characterized by different average Raman spectra, which describe the organelles in the cell: nucleus, lipid droplets/endoplasmic reticulum (ER), cytoplasm, mitochondria, cell border and the outside of the cell. The colors of the clusters correspond to the colors of the Raman spectra of the nucleus (red), lipid droplets/ER (blue), oleic lipid droplets (orange), cytoplasm (green), mitochondria (magenta), cell border (light grey).

Number of analysed cells *n*(NHA) = 4, *n*(NHA with all-*trans*-retinal) = 16, *n*(CRL-1718) = 4, *n*(CRL-1718 with all-*trans*-retinal) = 16, *n*(U-87 MG) = 4 and *n*(U-87 MG with all-*trans*-retinal) = 16, number of control and incubated with all-*trans*-retinal Raman spectra used for averaging 18 125 and 15 525; 8325 and 6825; 8325 and 6825, respectively.

WITec Project Plus 4.1 software was used for the analysis of Raman data. Raman data were first pre-processed using: the cosmic rays removal method (model: filter size: 2, dynamic factor: 10), the smoothing procedure (Savitzky–Golay, order: 4, derivative: 0) and background subtraction. Then the Raman maps were created by the Cluster Analysis, which means that spectra were divided into groups based on similarity. Details were shown in previous works.[19,20] Finally Raman spectra were transported to Origin Pro 2021 for calculation *e.g.* mean ± SD, ANOVA and produce graphs. The statistical analysis of the spectroscopic data was conducted using the one-way analysis of variance (ANOVA) test within the OriginPro 2021 software. Subsequently, the Tukey test was employed to determine the statistical significance; the asterisk * denotes that the differences are statistically significant, *p*-value ≤ 0.05.

Results and discussion

To elucidate the involvement of all-*trans*-retinal in cancer, we conducted an *in vitro* study on brain cancer cells using Raman imaging. Here we focused first on information that could be extracted from Raman imaging of normal human astrocytes (NHA), astrocytoma (CRL-1718) and glioblastoma (U-87 MG) cells, and then we clarified the effect of supplementation cells by all-*trans*-retinal. We focused on the biochemical compositions of cellular organelles such as the lipid droplets, mitochondria, nuclei and cytoplasm. Astrocytes (NHA) are normal brain cells, astrocytoma (CRL-1718) is a mildly aggressive brain tumor and U-87 MG is a highly aggressive brain tumor.

Fig. 2 shows typical Raman images and spectra of NHA, CRL-1718 and U-87 MG cells. The Raman map of the whole cells and maps of particular organelles such as a nucleus (red), mitochondria (magenta), oleic lipid droplets (orange), lipid droplets/endoplasmic reticulum (blue), cytoplasm (green), cell membrane (light grey) are presented. The colors of Raman maps correspond to the colors of Raman spectra (400–1800 cm^{-1}).

Fig. 3 shows typical Raman images and spectra of supplemented NHA, CRL-1718 and U-87 MG with 1 μM of all-*trans*-retinal for 24 hours (left part) and 10 μM of all-*trans*-retinal for 48 hours (right part), two different boundary points – the lowest concentration with the shortest time and the highest concentration with the longest time of incubation.

The results presented in Fig. 2 and 3 confirm that Raman imaging is an appropriate tool for qualitative and semi-quantitative analysis of the single human brain cell composition. Raman spectra of human brain cells are dominated by bands position at 750, 1003, 1126, 1254, 1310, 1337, 1444, 1583 and 1654 cm^{-1}. The strongest Raman signals at 1003, 1254, 1444 and 750, 1003, 1126, 1310, 1337, 1583, 1654 are contributed to Raman bands of lipids and proteins, respectively. Bands marked on green (Fig. 2 and 3) at 750, 1126, 1310, 1337 and 1583 cm^{-1} perfectly correspond to the Raman vibrations of cytochrome *c*.[19] Detailed Raman band assignments presented in Fig. 2 and 3 are presented in Table 1.

As we can see from Fig. 2 and 3 Raman spectra differ depending on the supplementation. There are differences in the presence of particular bands, for example, the band 750 cm^{-1} cannot be seen in the cell nucleus and cell membrane. To clarify the differences resulting from cell supplementation we presented the mean and difference spectra of selected organelles in Fig. 4 – lipid droplets/ER, Fig. S1† – mitochondria, Fig. S2† –

Table 1 Raman vibrational mode assignments for the identified bands[21–32]

Raman band wavenumber [cm^{-1}]	Raman vibrational mode assignment[21–32]
750	Heme group vibration/symmetric vibrations of pyrrole rings in cytochrome *c* and *b*
1003	Phenylalanine/lipids/proteins
1092	Fatty acids
1126	Vibrations of C_b–CH_3 side radicals/cytochrome *c*
1248	Methine bridges (bonds $C_\alpha C_\mu$, $C_\alpha C_\mu H$) cytochrome *c*
1254	Amide III in proteins/tryptophan/DNA/RNA bases/lipids
1310	Amide III in lipids/vibrations of all heme bonds/cytochrome *c*
1337	Proteins/cytochrome *c*
1363	Mode ν_4, methine bridges (bonds $C_\alpha C_\mu$, $C_\alpha C_\mu H$) cytochrome *c*
1444	CH_2 and CH_3 deformation/lipids/fatty acids/cholesterol
1583	Cytochrome *c*
1634	Methine bridges (bonds $C_\alpha C_\mu$, $C_\alpha C_\mu H$) cytochrome *c*
1654	C=O amide I in proteins/C=O stretching in lipids/fatty acids

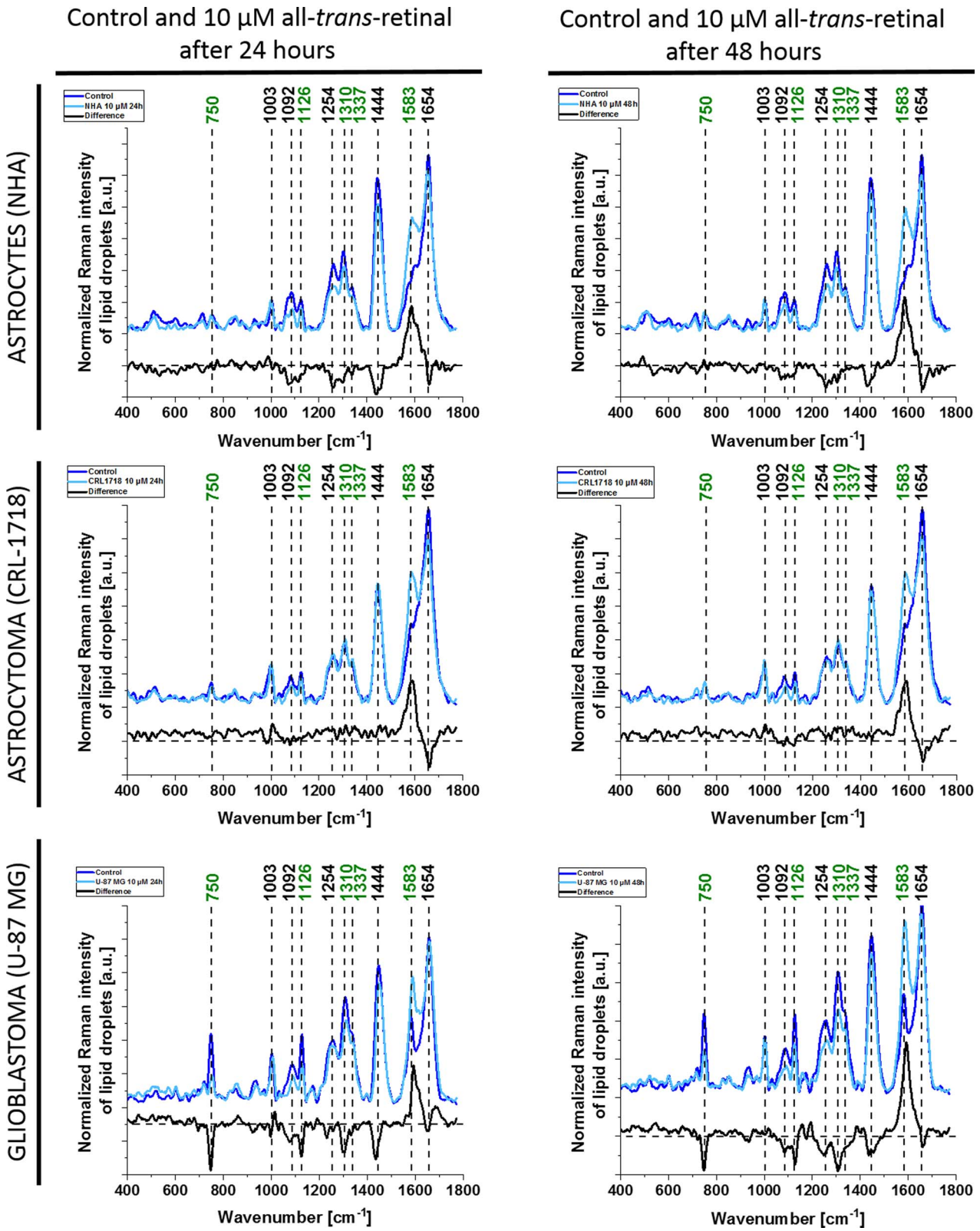

Fig. 4 Average and difference spectra for cell lipid droplets/ER from NHA, CRL-1718 and U-87 MG cell lines, control and supplemented with 10 μM all-*trans*-retinal of two incubation times: 24 (left) and 48 (right) hours. Dark blue – average from control cells, light blue – average from cells supplemented with 10 μM all-*trans*-retinal, black – difference spectrum (supplemented – control).

nucleus and Fig. S3† – cytoplasm. For each line of the human brain cells, a comparison between Raman spectra of control cells and supplemented cells with a concentration of 10 μM all-*trans*-retinal at two incubation times (24 and 48 hours) is presented.

From Fig. 4 we can see that as a result of supplementation with all-*trans*-retinal for 24 and 48 hours, we observe an increase of the Raman band at around 1583 cm^{-1}. The band corresponds to the methine bridge vibration of cytochrome *c*. A detailed analysis of observed Raman bands of cytochrome *c* has been provided later in this work. For astrocytes (NHA) and glioblastoma (U-87 MG) we observe also an appearance of the Raman bands at 776, 834, 951, 988, 1152, 1218, 1538, 1585, 1610, 1638 cm^{-1} and 447, 504, 655, 679, 794, 860, 1015, 1143, 1163, 1193, 1276, 1386, 1563, 1592, 1612, 1672–1696 cm^{-1}, respectively. For NHA and U-87 MG we see a clear disappearance of the Raman bands at 712, 873, 930, 1040, 1074, 1112, 1260, 1300, 1338, 1438, 1455, 1660 cm^{-1} and 694, 747, 922, 971, 996, 1029, 1077, 1124, 1174, 1230, 1256, 1302, 1651, 1736 cm^{-1}, respectively. We do not observe such clear changes for the astrocytoma (CRL-1718) however Raman bands at 768, 823, 851, 956, 1006, 1157, 1190, 1238, 1261, 1289, 1311, 1349, 1391, 1418, 1455, 1475, 1504, 1557, 1590, 1707, 1740 appeared and disappeared at 984, 1056, 1081, 1660 cm^{-1}. The Raman band at around 750 cm^{-1} is also interesting, its disappearance is most visible in the most aggressive brain cell line (U-87 MG). An analogous analysis was conducted on mitochondria, nucleus and cytoplasm, and the results are presented in Fig. S1–S3,† respectively. Comparable Raman bands changes were observed during our investigation. The results are similar to those in lipid droplets presented in Fig. 4. Incubating brain normal and cancer cells with all-*trans*-retinal leads to a notable increase in Raman signal for the ν_{19} vibration mode corresponding to cytochrome *c* (band at 1583 cm^{-1}).

Allow us to provide a clear explanation of the observed shifts in the redox status of cytochrome *c* within an individual human brain cell. In Fig. 2–4 and S1–S3,† the Raman bands of cytochrome *c* that undergo resonance Raman enhancement in brain cell lines are depicted in green. Four prominent peaks of cytochrome at 750 (symmetric vibrations of pyrrole rings), 1126 (vibrations of C_b–CH_3 side radicals), 1310 (vibrations of all heme bonds), 1363 (mode ν_4) and 1583 cm^{-1} (ν_{19} mode, vibrations of methine bridges ($C_\alpha C_\mu$, $C_\alpha C_\mu H$ bonds) and the $C_\alpha C_\beta$ bond) are discernible (Fig. 5). Other Raman bands at 1248, 1363 and 1634 cm^{-1}, corresponding to methine bridges (bonds $C_\alpha C_\mu$, $C_\alpha C_\mu H$), also exhibit lower intensities. The Raman signals of the reduced form of cytochrome *c* exhibit increased intensities (presented in Fig. 5). In our analysis of the brain cell lines, we utilized the 1583 cm^{-1} vibrational mode (ν_{19}) as an indicative Raman band for ferrous cytochrome *c*, as shown in Fig. 2–4 and S1–S3.† Despite the existence of several overlapping bands in that specific region: ν_{19} of ferric heme *c* (1582 cm^{-1}), ν_{19} of ferrous heme *c* (1582 cm^{-1}), ν_2 of ferric heme *c* (1585 cm^{-1}), ν_{19} of ferrous heme *b* (1586 cm^{-1}) and ν_2 of ferrous heme *b* (1583 cm^{-1}) we can eliminate from our discussion all ferric modes because the absolute resonance Raman intensities of the ferric modes are very weak in comparison to the ferrous bands

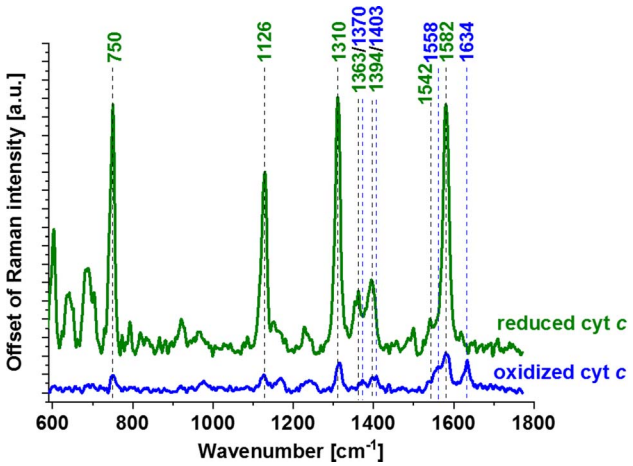

Fig. 5 Raman spectra of cytochrome *c* solutions (0.23 mM) in ferric (oxidized, Fe^{3+}) and ferrous (reduced, Fe^{2+}) forms dissolved in potassium phosphate buffer pH = 7.4, cuvette optical path 1 cm. Ferrous cytochrome *c* was prepared by adding a tenfold excess of reducing agent $NaBH_4$.

except the band 1634 cm^{-1} corresponding to the ferric cytochrome *c*. Consequently, the Raman bands at 1583 cm^{-1} (associated with the reduced form) and at 1634 cm^{-1} (associated with the oxidized form) of cytochrome *c* can serve as pivotal factors for monitoring the reduction level in brain cells.

Summarising the analysis of the presented difference spectra so far, we concluded that the most significant differences are observed for the U-87 MG cell line and the least for the NHA. The main differences occurred for the Raman bands at 750, 1254, 1310, 1444, 1583 and 1654 cm^{-1}. These bands correspond as follows: 750 cm^{-1} – cytochrome *c* and *b*, 1254 cm^{-1} – amide III in proteins, 1310 cm^{-1} – amide III/lipids, 1444 cm^{-1} – CH deformations/lipids, 1583 cm^{-1} – cytochrome *c* and 1654 cm^{-1} – amide I in proteins.[21,31] It may indicate that the supplementation of all-*trans*-retinal results in cellular changes in the level of lipids and proteins. Moreover, a significant difference in the amount of cytochrome *c* has been observed for each analyzed cell line, which means that all-*trans*-retinal influences the cytochrome *c* redox status in cells. Our presented Raman data shows that the biochemical composition of normal brain cells (astrocytes) is different than astrocytoma and glioblastoma both without and supplemented with all-*trans*-retinal. It means that depending on the aggressiveness, cells use all-*trans*-retinal in different ways in their physiology.

For a deeper understanding of alterations post-supplementation, ANOVA analysis was employed to discern whether the analyzed Raman data exhibited significant differences. Statistically significant changes have been seen for the cell lines after 24 and 48 hours of supplementation (Fig. 6). We believe that the observations of biomolecule variation over time that were formed after supplementation with all-*trans*-retinal might be utilized in metabolic processes and removed from the cell or transformed into other compounds.

Fig. 4 and S1–S3† highlight the most prominent differences in mitochondria, nucleus, lipid droplets and cytoplasm, prompting their selection for subsequent ANOVA analysis.

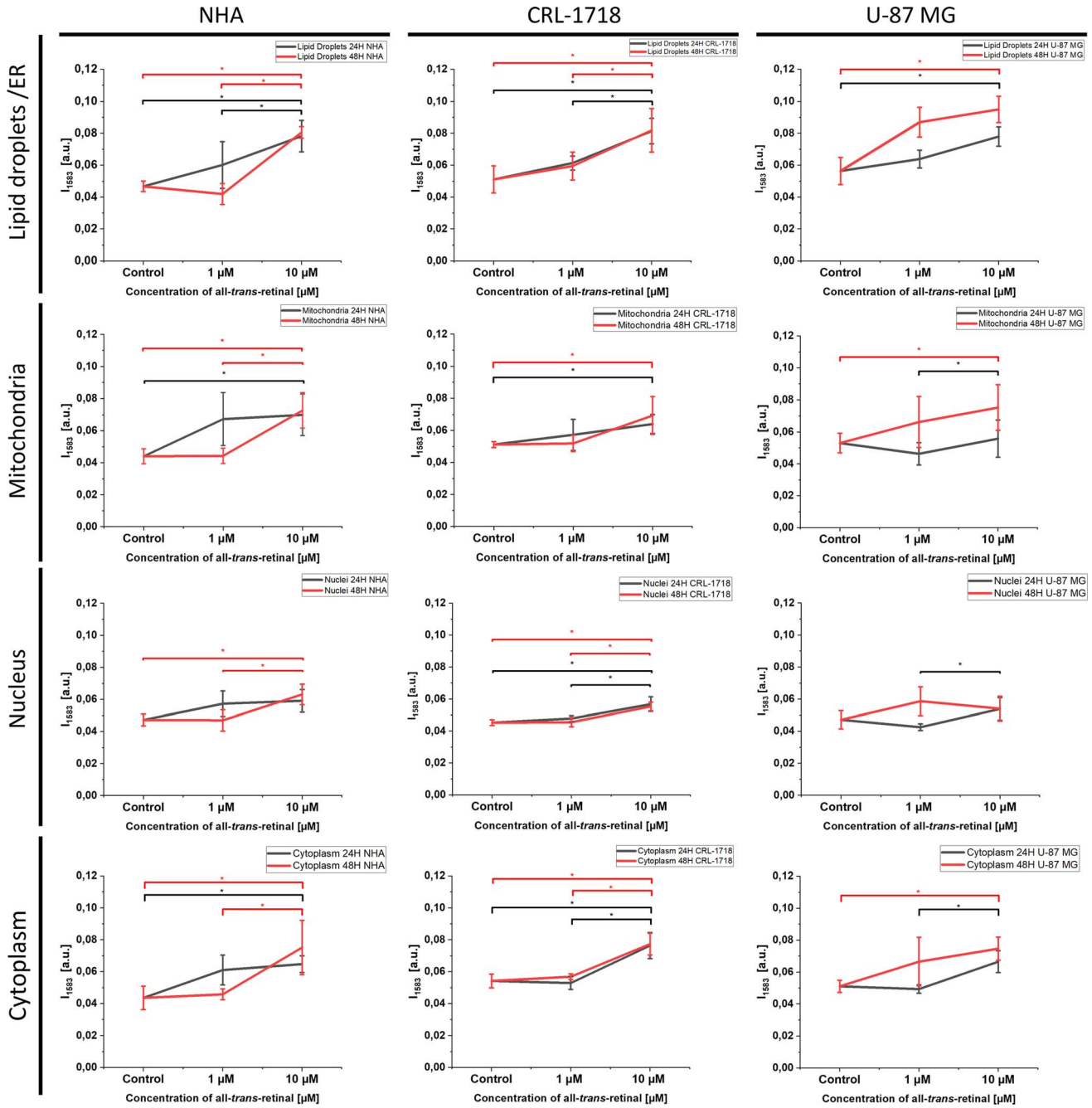

Fig. 6 Differences in the Raman band 1583 cm^{-1} peak intensity and standard deviation (SD) for lipid droplets/ER, mitochondria, nucleus and cytoplasm in NHA, CRL-1718 and U-87 MG cell lines. Points represent control (unsupplemented cells), cells supplemented with 1 μM and 10 μM. The black line refers to supplementation for 24 hours and the red line refers to supplementation for 48 hours.

Fig. 6 illustrates the ANOVA results for NHA, CRL-1718, and U-87 MG cell lines for the 1583 cm^{-1} band. The depicted results encompass control (unsupplemented cells), 1 μM, and 10 μM of all-*trans*-retinal for 24 hours (black line) and 48 hours (red line).

As we can see in Fig. 6 an increase of Raman band intensity of reduced form of cytochrome *c* (1583 cm^{-1}) is observed with increasing concentration of all-*trans*-retinal. Most observations are statistically significant.

Our results of the current study demonstrated that treated brain tumor cells with all-*trans*-retinal deregulate cell cycle and these changes might be monitored by Raman imaging. Our previous studies[17,18] reported that retinoids such as retinoic acid, retinol and retinyl palmitate have an impact on the redox status of cytochrome *c* in cancers, particularly in breast and lung cancers. Notably, all-*trans*-retinoic acid plays an important role in differentiation and apoptosis with the activation of TNF-a and caspase-8 pathways.[33] Karmakar *et al.* showed that combination therapy (all-*trans*-retinoic acid with paclitaxel) of human glioblastoma (U-87 MG) xenografts induced the mitochondria-mediated pathway of apoptosis with an increase

in the Bax : Bcl-2 ratio and mitochondrial release of cytochrome *c* and Smac/Diablo into the cytosol. In addition, combination therapy promoted phosphorylation of Bcl-2 for its inactivation and down-regulated NF-kB and BIRC proteins, indicating suppression of several cell survival factors.[33] Our results of glioblastoma (mitochondria) presented in Fig. S1† confirm a release of cytochrome *c* (negative contributions in the difference spectrum) at the first 24 hours of supplementation with all-*trans*-retinal, which is consistent with Karmakar's observation. It is also interesting that the increase of Raman bands intensity at approximately 1580–1590 cm^{-1} may indicate not only the level of redox status of cytochrome *c*[18] but also the increase in protein phosphorylation[20] or metabolism of all-*trans*-retinal to retinol (retinol is characterized by a strong Raman band at 1590 cm^{-1}, Fig. 1B). A visible Raman shift to 1590 cm^{-1} is observed in the difference Raman spectra of glioblastoma lipid droplets and cytoplasm after 48 hours of supplementation. We should also consider the second scenario where the presence of cytochrome results in the conversion of retinal to retinoic acid, which is required for growth and development in the human body.[12] Altucci and Gronemeyer have proven that retinoids express antitumour activity due to retinoic acid interruption of particular steps in carcinogenesis.[34] The findings align with our XTT results (data not shown), indicating that once a specific threshold of all-*trans*-retinal concentration (around 25 μM) is surpassed, cell death occurs. According to Bushe and Wan's results, fenretinide and isotretinoin as an isomer of retinoic acid are considered as an agents which generate reactive oxygen species (ROS) and decrease cyclin B1 and Bcl-2 expressions in brain cancer.[31] It indicates that all-*trans*-retinal as a compound from retinoid group might be an anti-cancer agent. Differences in cytochrome *c* levels point to the possibility that the presence of all-*trans*-retinal may influence different metabolic pathways, potentially playing a role in the inhibition of cancer development and progression. This manuscript presents an original study by using Raman imaging to track changes in the redox status of mitochondrial cytochromes, proposing it as a competitive clinical diagnostic tool for cancer diseases associated with mitochondrial dysfunction. A thorough understanding of how cytochromes influence metabolic dysregulation requires future analyses involving biological validation assays.

Conclusions

In this study, we investigated the hypothesis on impact of reduction–oxidation pathways induced by all-*trans*-retinal associated with cytochrome *c* in the progression of brain cancer. We have used Raman imaging as a label-free method for tracking the metabolism of all-*trans*-retinal in human normal astrocytes and cancerous brain cells of different aggressiveness. Raman microspectroscopy can track changes at the level of specific cellular organelles. We have shown that the biochemical composition of normal brain cells (astrocytes) is different than that of astrocytoma and glioblastoma both without and supplemented with all-*trans*-retinal. It means that depending on aggressiveness, cells use all-*trans*-retinal in different ways in their biological activity. It was evident from our study that all-*trans*-retinal has a profound impact on the mitochondrial functional activity (redox status) of the brain cancer cells that was monitored using Raman imaging. Our results confirmed that the human brain cancer cells demonstrate alterations in redox status compared to normal cells. The correlation has been established between the intensity of reduced form of cytochrome *c* Raman band at 1583 cm^{-1} and the malignancy grade in brain cancer cells. Further research using advanced molecular biology techniques is needed to fully support the hypothesis confirmed by Raman results presented in this paper that the shift from the oxidized Fe^{3+} to the reduced Fe^{2+} form carries notable implications in electron transport chain, oxidative phosphorylation and apoptosis.

Author contributions

Conceptualization: K. J., J. S., M. K., H. A.; investigation: K. J.; methodology: J. S.; writing – original draft: K. J., J. S.; manuscript editing: J. S., K. J.; manuscript revision: J. S., M. K., K. J.; funding: H. A. All authors have read and agreed to the published version of the manuscript.

Conflicts of interest

There are no conflicts of interest to declare.

Acknowledgements

This work was supported by the National Science Centre of Poland (OPUS, UMO-2021/43/B/ST4/01547). This paper has been completed while the first author was the Doctoral Candidate in the Interdisciplinary Doctoral School at the Lodz University of Technology, Poland.

References

1 Worldwide cancer data | World Cancer Research Fund International, https://www.wcrf.org/cancer-trends/worldwide-cancer-data/, accessed February 28, 2024.
2 M. Bredel, *Lancet Oncol.*, 2003, **4**, 257–258.
3 S. Marie, *Clinics*, 2011, **66**(Suppl 1), 33–43.
4 Y.-E. L. Koo, G. R. Reddy, M. Bhojani, R. Schneider, M. A. Philbert, A. Rehemtulla, B. D. Ross and R. Kopelman, *Adv. Drug Delivery Rev.*, 2006, **58**, 1556–1577.
5 K. H. Dragnev, J. R. Rigas and E. Dmitrovsky, *Oncologist*, 2000, **5**, 361–368.
6 R. Rühl, *Proc. Nutr. Soc.*, 2007, **66**, 458–469.
7 C. Aleksandra, *Proc. Nutr. Soc.*, 2018, **7**, 371.
8 J. von Lintig, *J. Biol. Chem.*, 2012, **287**, 1627–1634.
9 G. H. Travis, M. Golczak, A. R. Moise and K. Palczewski, *Annu. Rev. Pharmacol. Toxicol.*, 2007, **47**, 469–512.
10 J. L. Napoli and K. R. Race, *J. Biol. Chem.*, 1988, **263**, 17372–17377.
11 A. Lindqvist and S. Andersson, *J. Biol. Chem.*, 2002, **277**, 23942–23948.

12 H. Marona, A. Gunia and E. Pękala, Retinoidy – rola w farmakoterapii w aspekcie komórkowego mechanizmu działania, *Terapia i leki*, 2010, vol. 66, issue 3, **https://ptfarm.pl/pub/File/Farmacja%20Polska/2010/03-2010/06%20%20Retinoidy.pdf**.
13 S. Stewart, R. J. Priore, M. P. Nelson and P. J. Treado, *Annu. Rev. Anal. Chem.*, 2012, **5**, 337–360.
14 S. P. Mulvaney and C. D. Keating, *Anal. Chem.*, 2000, **72**, 145–158.
15 L. A. Lyon, C. D. Keating, A. P. Fox, B. E. Baker, L. He, S. R. Nicewarner, S. P. Mulvaney and M. J. Natan, *Anal. Chem.*, 1998, **70**, 341R–361R.
16 J. Surmacki, B. Brozek-Pluska, R. Kordek and H. Abramczyk, *Analyst*, 2015, **140**, 2121–2133.
17 H. Abramczyk and J. M. Surmacki, *Cancers*, 2023, **15**, 4535.
18 J. M. Surmacki and H. Abramczyk, *Sci. Rep.*, 2023, **13**, 15049.
19 H. Abramczyk, B. Brozek-Pluska and M. Kopeć, *Sci. Rep.*, 2022, **12**, 2120.
20 H. Abramczyk, A. Imiela, B. Brożek-Płuska, M. Kopeć, J. Surmacki and A. Śliwińska, *Cancers*, 2019, **11**, 2017.
21 A. Rygula, K. Majzner, K. M. Marzec, A. Kaczor, M. Pilarczyk and M. Baranska, *J. Raman Spectrosc.*, 2013, **44**, 1061–1076.
22 M. Kopeć, K. Beton, K. Jarczewska and H. Abramczyk, *Sci. Rep.*, 2022, **12**, 18561.
23 J. M. Surmacki, I. Quiros-Gonzalez and S. E. Bohndiek, *Antioxidants*, 2022, **11**, 573.
24 P. T. W. Jr, C. Zhang, F. Vesuna, J. W. Kang, J. Garry, R. R. Dasari, I. Barman and V. Raman, *Oncotarget*, 2017, **8**, 20266–20287.
25 H. N. Banerjee, A. Banerji, A. N. Banerjee, E. Riddick, J. Petis, S. Evans, M. Patel, C. Parson, V. Smith, E. Gwebu and S. Voisin, *J. Cancer Sci. Ther.*, 2015, **7**, 44–47.
26 Z. Movasaghi, S. Rehman and I. U. Rehman, *Appl. Spectrosc. Rev.*, 2007, **42**, 493–541.
27 H. Georg Schulze, S. O. Konorov, J. M. Piret, M. W. Blades and R. F. B. Turner, *Analyst*, 2013, **138**, 3416–3423.
28 H. Abramczyk, J. M. Surmacki, B. Brozek-Pluska and M. Kopec, *Cancers*, 2021, **13**, 2599.
29 H. Abramczyk and A. Imiela, *Spectrochim. Acta, Part A*, 2018, **188**, 8–19.
30 N. Stone, C. Kendall, J. Smith, P. Crow and H. Barr, *Faraday Discuss.*, 2004, **126**, 141–157.
31 N. Bushue and Y.-J. Y. Wan, *Adv. Drug Delivery Rev.*, 2010, **62**, 1285–1298.
32 J. De Gelder, K. De Gussem, P. Vandenabeele and L. Moens, *J. Raman Spectrosc.*, 2007, **38**, 1133–1147.
33 S. Karmakar, N. L. Banik and S. K. Ray, *Cancer*, 2008, **112**, 596–607.
34 L. Altucci and H. Gronemeyer, *Nat. Rev. Cancer*, 2001, **1**, 181–193.